Vacuum 168 (2019) 108850

Contents lists available at ScienceDirect

Vacuum

journal homepage: www.elsevier.com/locate/vacuum

High-entropy oxide thin films based on Al–Cr–Nb–Ta–Ti

Alexander Kirnbauer[a,*], Christoph Spadt[a], Christian M. Koller[a,b], Szilard Kolozsvári[c], Paul H. Mayrhofer[a]

[a] Institute of Materials Science and Technology, TU Wien, Getreidemarkt 9, 1060, Vienna, Austria
[b] Pankl Systems Austria GmbH, Engine Systems, Kaltschmidstrasse 2-6, 8600, Bruck an der Mur, Austria
[c] Plansee Composite Materials GmbH, Siebenbürgerstrasse 23, 86983, Lechbruck am See, Germany

ARTICLE INFO

Keywords:
High-entropy alloys (HEAs)
Reactive sputtering
Multi-element oxides

ABSTRACT

Single-phase crystalline (Al,Cr,Nb,Ta,Ti)O_2 high-entropy oxide thin films were synthesized at 400 °C by reactive magnetron sputtering of an equimolar Al–Cr–Nb–Ta–Ti-compound target. These show similar chemistry as well as the same rutile structure, even when varying the relative oxygen flow-rate ratio (f_{O2}) during deposition over a wide range. Upon increasing f_{O2} from 30 to 80%, their hardness increases from 22 to 24 GPa and their indentation moduli increased from 380 to 410 GPa. The materials stayed single-phase crystalline with the rutile structure during vacuum annealing up to 1200 °C, only their orientation changed from random-like to highly 101-textured.

The development and continuous improvement of materials able to withstand high temperatures and mechanical loads – allowing for an increased machining tool and component lifetime – is an everlasting topic. Protecting such components with thin hard coatings has become a common strategy to (partly) achieve this task. Among the reams of available materials or material combinations, binary or ternary transition metal nitrides (TMNs) such as Ti–Al–N, Ti–Al–Ta–N, or Cr–Al–N, belong to the most important and widely applied protective coatings. This is also because the structure of these nitrides is relatively stable with respect to changes in deposition parameters, which always vary when considering the 3D geometry of tools and components. To further improve the nitrides, especially with respect to thermal stability and oxidation resistance (unfortunately, the addition of Al is limited by the concomitant promotion of the unwanted hexagonal phase [1]), elements such as Ta, Zr or lanthanoids are added [2–9]. The preparation of hard and wear-resistant oxides such as α-Al_2O_3 is more complicated, especially at relatively low deposition temperatures (such as below 500 °C) [10,11]. In the case of Al_2O_3 – when aiming for a crystalline α-structured solid solution – the addition of α-stabilizing elements and the oxygen flow rate play a major role [12–16]. Also for other physical vapor deposition (PVD) synthesized oxides like TiO_2, a strong dependence on deposition parameters is reported, because TiO_2 easily grows amorphous or in the metastable anatase structure if substrate temperatures and/or oxygen flow ratios are not optimized [17].

Cantor et al. introduced a new alloying concept by mixing at least five principal elements, to develop equiatomic multicomponent alloys [18]. They investigated alloys composed of up to 20 elements with equiatomic composition. All these alloys were multi-phased, constituting of a predominant face-centred cubic (fcc) structure (mostly based on transition metals, notably Cr, Mn, Fe, Co and Ni) and interdendritic phases containing the other elements. Based on these results, so called high-entropy alloys (HEAs) or multiprincipal-element alloys were introduced by Yeh et al. [19–22]. Alloys can be defined as HEAs, when consisting of at least five principal elements (leading to a high configurational entropy) and forming simple structures like fcc, body-centred cubic (bcc), or hexagonal close-packed (hcp). The four core effects in HEAs – high-entropy, severe lattice distortion, sluggish diffusion, and the cocktail-effect – should lead to outstanding properties, like enhanced hardness, toughness, and thermal stability, when compared with conventional alloys, which in contrast are based on one or two principal elements [23].

Yeh et al. were also among the first to prepare nitride coatings based on the high-entropy concept, studying the material system Al–Cr–Ta–Ti–Zr intensively [24–27]. An increased bending strain was recently reported for Si-containing high-entropy nitride coatings [28], proofing the potential of the high-entropy concept. Later than the nitrides, multi-element oxides based on Al–Cr–Ta–Ti–Zr synthesised by reactive DC magnetron sputtering [29] were studied, yet these were amorphous in the as-deposited state and became multi-phased crystalline after annealing. Ceramic materials (like nitrides, oxides, carbides, and borides) are typically considered high-entropy, if they are single-phased and composed of at least five corresponding binary nitrides,

* Corresponding author.
E-mail address: alexander.kirnbauer@tuwien.ac.at (A. Kirnbauer).

https://doi.org/10.1016/j.vacuum.2019.108850
Received 17 June 2019; Received in revised form 25 July 2019; Accepted 27 July 2019
Available online 01 August 2019
0042-207X/

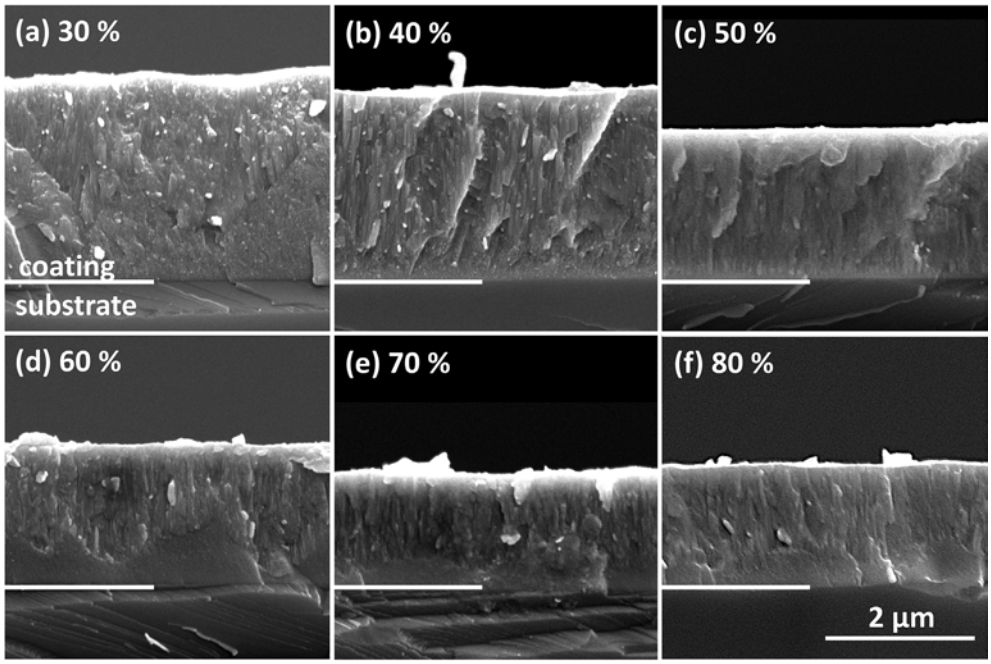

Fig. 1. SEM fracture cross-sections of our $(Al_{0.19}Cr_{0.13}Nb_{0.19}Ta_{0.30}Ti_{0.19})O_2$ coatings (on Si substrates) prepared with different oxygen flow-rate ratios f_{O2} of **(a)** 30%, **(b)** 40%, **(c)** 50%, **(d)** 60%, **(e)** 70%, and **(f)** 80%. The horizontal white line, indicating the interface between substrate and thin film, is as long as the 2-µm-scale bar.

oxides, carbides, and borides, respectively, having an entropy S ≥ 1.5R (with R being the ideal gas constant) [30,31]. In this regard also several high-entropy bulk oxides with different crystal structures (rock-salt, fluorite-type, perovskite-type) were investigated showing a high-entropy stabilization [32–34].

Here, we show results of high-entropy oxides synthesised by reactive pulsed-DC magnetron sputtering of a single compound-target composed of 20 at.% Al, Cr, Nb, Ta, and Ti. We aimed for a crystalline solid solution motivated by the fact that PVD allows for high cooling rates [35,36] and all elements except Al can form rutile-structured oxides (having the rutile structure at least as a metastable phase present). The morphology, structure, mechanical properties (indentation hardness, H, and elastic modulus, E), as a function of the relative oxygen flow rate ratio (f_{O2}) used will be discussed, as well as the thermal stability of the coating prepared with the highest f_{O2} of 80%, which was also the hardest in the as-deposited state.

Various Al–Cr–Nb–Ta–Ti–O coatings were deposited on polished 100-oriented Si ($20 \times 7 \times 0.38\,mm^3$) and $1\bar{1}02$-oriented sapphire ($10 \times 10 \times 0.53\,mm^3$) substrates by pulsed-DC (pulse frequency of 50 kHz and pulse length of 496 ns) magnetron sputtering of a powder-metallurgically prepared $Al_{0.2}Cr_{0.2}Nb_{0.2}Ta_{0.2}Ti_{0.2}$ target (Plansee Composite Materials GmbH) employing a modified Leybold Heraeus Z400 deposition system. The base pressure was below 0.3 mPa ($3{\cdot}10^{-6}$ mbar) and the substrate-to-target distance (in a face-to-face arrangement) was 4 cm. The relative oxygen flow-rate ratio [$f_{O2} = F_{O2}/(F_{O2}+F_{Ar})$, with F_{O2} and F_{Ar} being the flow rate of O_2 and Ar, respectively] was varied between 30 and 80% – at a slightly varying process pressure of 0.43–0.46 Pa, respectively – to obtain its influence on the coating's structure and mechanical properties. Other than that, the temperature and bias potential applied to the substrates was always 400 °C and −50 V, respectively, and the deposition time was 110 min. The 75-mm-diameter target was operated with a constant current of 0.5 A, leading to a power density of around 5.4 W/cm^2. Fracture cross-sections of the coatings (on Si substrates) were investigated by scanning electron microscopy (SEM) using a FEI Quanta SEM equipped with a field emission gun (FEG) to obtain growth morphology and coating thickness. Their chemical compositions were obtained by energy dispersive X-ray spectroscopy (EDS), where the quantification of oxygen was obtained by Fe_2O_3 calibration standards. Detailed transmission electron microscopy (TEM, using a FEI TECNAI F20) was conducted of the coating (on sapphire substrate) prepared with f_{O2} of 70%. The selected area electron diffraction (SAED) pattern was evaluated using GATAN Microscopy Suite 3.

With respect to structure investigations, X-ray diffraction (XRD) patterns were collected with Bragg-Brentano geometry employing a PANalytical XPert Pro MPD (θ-θ diffractometer) equipped with a Cu-Kα source (λ = 0.15408 nm, 45 kV and 40 mA). Vacuum annealing treatments of the coating (on sapphire substrate) prepared with the highest f_{O2} of 80% were carried out in a Centorr LF20-2000 vacuum furnace at T_a = 800, 900, 1000, 1100, and 1200 °C with 10 min holding time at peak temperature (the heating rate was 20 K/min and the cooling rate was at least 50 K/min down to 200 °C). Indentation hardness, H, and elastic modulus, E, of the coatings on sapphire substrates were obtained by analysing the load-displacement curves of nanoindentation measurements using an UMIS II nanoindenter, according to the procedure by Oliver and Pharr [37].

All coatings prepared contain about 64–65 at.% oxygen, thus nearly MeO_2 stoichiometry, regardless of the relative oxygen flow-rate ratio used (which was between 30 and 80%). Also the content of the metal elements is within the error of measurements, being about 11 at% for Ta, about 7 at% for Al, Nb, and Ti, and about 5 at% for Cr. Consequently, these coatings correspond to $(Al_{0.19}Cr_{0.13}Nb_{0.19}Ta_{0.30}Ti_{0.19})O_2$, when using the MeO_2 nomenclature.

Other than the chemistry, the growth morphology shows a dependence on the relative oxygen flow-rate ratio f_{O2} used. Coatings deposited with f_{O2} = 30% show an initially dense and feature-less structure near the substrate, which changes to a more columnar-like growth after 300–500 nm film thickness, Fig. 1a. A similar growth morphology shows the coating processed with f_{O2} = 40%, Fig. 1b. However, the initially feature-less structure changes already after 200 nm film thickness towards a columnar growth-morphology, and the overall thickness slightly decreased to 2.5 µm. Further increasing f_{O2} to 50% further decreases the thickness-range of the feature-less structure (close to the substrate), as well as the overall coating thickness, Fig. 1c.

The feature-less region close to the substrate is still present for f_{O2} = 60%, changing to columnar structure with increasing film

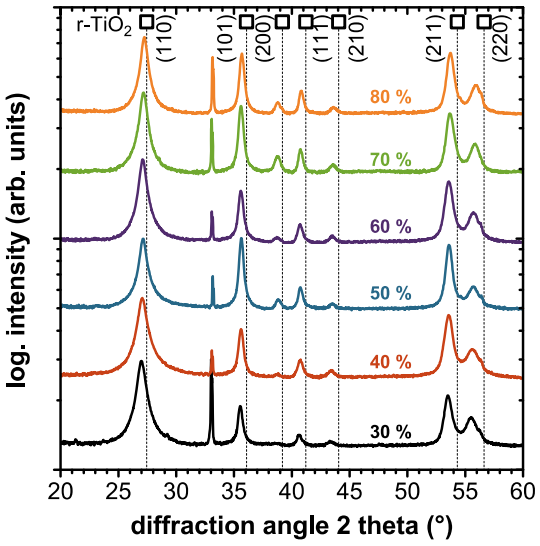

Fig. 2. XRD patterns of our $(Al_{0.19}Cr_{0.13}Nb_{0.19}Ta_{0.30}Ti_{0.19})O_2$ coatings on Si substrates, grown with different f_{O2} between 30 and 80% (the XRD patterns are labelled with the corresponding f_{O2}). The small and sharp XRD peak at 2θ ~33° stems from the Si substrate. All coatings exhibit only one crystalline phase, being of the rutile-type (the positions for rutile TiO_2, r-TiO_2, obtained from ICDD #01-073-1782, are indicated).

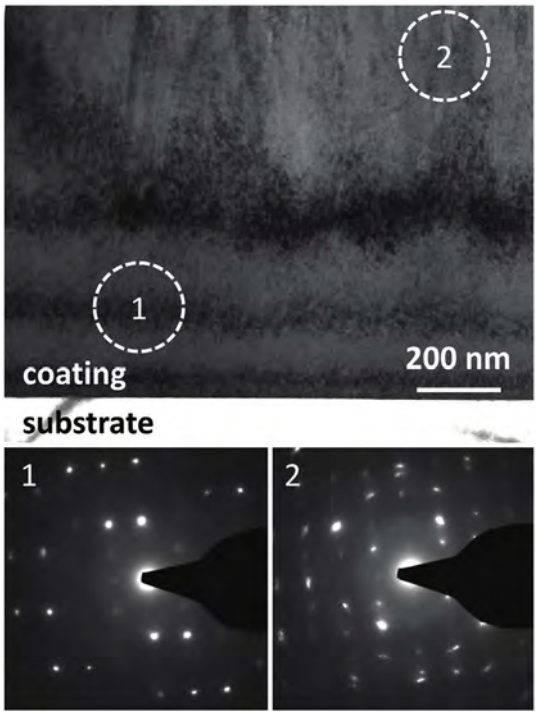

Fig. 3. Cross-sectional bright-field TEM of the $(Al_{0.19}Cr_{0.13}Nb_{0.19}Ta_{0.30}Ti_{0.19})O_2$ coating (on sapphire substrate) prepared with f_{O2} = 70% in its as-deposited state. The SAED of the region close to the substrate indicates a highly oriented rutile structure with discrete diffraction spots (inset 1) whereas the region above provides small variations in the orientation leading to more streak-like diffraction (inset 2).

thickness, Fig. 1d. But the columns of this coating grow with a denser morphology and also the overall film thickness further decreases, due to a higher poisoning-state of the target. Coatings prepared with f_{O2} = 70 and 80%, Fig. 1e and f, still exhibit the glossy-like appearance at the interface (where actually, transmission electron microscopy showed a highly oriented crystal growth), followed by a more columnar-like growth morphology (corresponding to those obtained by a competitive growth of different-oriented crystals). These coatings have almost the same thickness of 1.6 μm, being slightly below that obtained for f_{O2} = 60%.

All coatings prepared exhibit only one crystalline phase, being a rutile-type solid solution. Their XRD peak shape is nearly independent on the f_{O2} used, Fig. 2. Rietveld analysis (using Si standards to minimize measurement errors) leads to lattice parameters of a = 4.67 Å and c = 3.01 Å for the coating prepared with f_{O2} = 30%. These are larger than the TiO_2 reference (ICDD #01-073-1782) having a = 4.593 Å and c = 2.959 Å. The coatings prepared with f_{O2} = 40, 50, and 60% exhibit lattice parameters of a = 4.67, 4.67, and 4.68 Å and c = 3.00, 3.01, and 3.01 Å, respectively. Coatings prepared with the highest oxygen flow-rate ratios (f_{O2} = 70 and 80%) show a slightly smaller a lattice parameter of 4.66 Å, combined with c = 3.01 Å. Consequently, the structure, the lattice parameters and the corresponding cell volume (with $V = a^2 \times c$ of the tetragonal rutile structure), with 65.66, 65.60, 65.71, 65.76, 65.36, and 65.21 $Å^3$, are nearly independent on the relative oxygen flow-rate ratio of 30, 40, 50, 60, 70, and 80% used during deposition, respectively. The biaxial compressive stresses of the coatings (obtained by the substrate curvature method) are about −1 GPa when prepared with f_{O2} = 30 and 40%, and about −2 GPa when prepared with higher relative oxygen flow-rate ratios. The configurational entropy of our $(Al_{0.19}Cr_{0.13}Nb_{0.19}Ta_{0.30}Ti_{0.19})O_2$ coatings can (due to their single-phase structure) be calculated to be 1.57R, thus clearly above the required 1.5R of high-entropy materials.

The clearly single-phase nature of our oxide coatings was also confirmed by detailed TEM and SAED investigations, showing no additional grain or column boundary phases. Exemplarily, Fig. 3 shows the cross-sectional TEM and SAED of the $(Al_{0.19}Cr_{0.13}Nb_{0.19}Ta_{0.30}Ti_{0.19})O_2$ coating prepared with f_{O2} = 70%. The growth morphology is feature-less close to the substrate and more columnar above this region, as already mentioned during discussing the SEM images (Fig. 1). SAED investigations show a single-phase rutile structure throughout the coating thickness with a high orientation in the feature-less region (on Si with its native SiO_2 surface as well as on sapphire substrates), see insets 1 and 2, respectively. Hence, we envision the highly oriented growth to be the reason for the feature-less appearance.

Corresponding to the chemical composition and crystal structure, also the indentation hardness and modulus, are similar for all coatings prepared. However, H as well as E slightly increase, from 22 to 24 GPa and from 380 to 400 GPa, respectively, with increasing oxygen flow-rate ratio, Fig. 4. This trend agrees with the growth morphology,

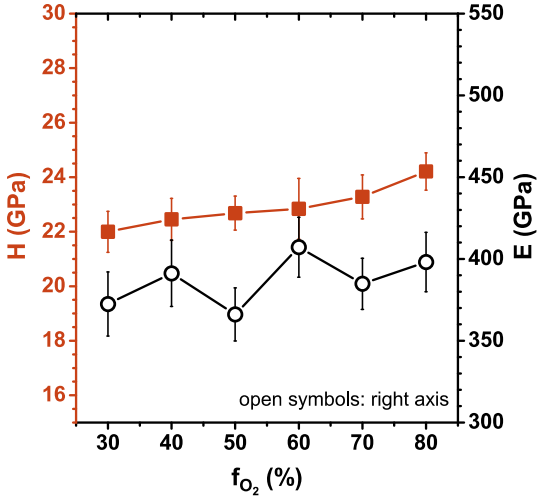

Fig. 4. Indentation hardness H and modulus E (open symbols, right axis) of our $(Al_{0.19}Cr_{0.13}Nb_{0.19}Ta_{0.30}Ti_{0.19})O_2$ coatings on sapphire substrates, prepared with oxygen flow-rate ratios f_{O2} of 30 till 80%.

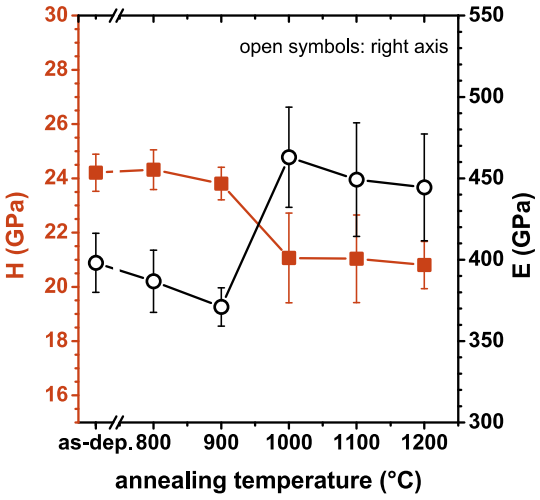

Fig. 5. Indentation hardness H and modulus E (open symbols, right axis) of our $(Al_{0.19}Cr_{0.13}Nb_{0.19}Ta_{0.30}Ti_{0.19})O_2$ coating (on sapphire substrate) prepared with f_{O2} = 80% in its as-deposited state and after vacuum annealing at T_a = 800 till 1200 °C (10 min holding time at the peak temperature).

becoming denser with increasing oxygen flow-rate ratio, compare with Fig. 1.

The coating with the highest hardness (24 GPa) in the as-deposited state (which was prepared with the highest oxygen flow-rate ratio of f_{O2} = 80%), still shows ~24 GPa even after vacuum annealing at 900 °C, Fig. 5. Annealing at T_a = 1000 °C caused the hardness to decrease to ~21 GPa, but even when raising T_a to 1200 °C, still 21 GPa are obtained.

The indentation modulus shows an opposite behaviour of nearly stable values up to T_a = 900 °C, with an increase from ~400 to 460 GPa when increasing T_a to 1000 °C, and again nearly stable values when T_a is raised further to 1200 °C. The rather distinct change in H and E when increasing T_a from 900 to 1000 °C, with nearly constant values for lower respectively higher temperatures (Fig. 5), basically stems from changes in average coherently diffraction domain sizes (CDS) and crystal orientation. Detailed XRD studies (not shown here) indicate an increase in CDS from ~4 to 30 nm and a change in crystal orientation from nearly random to highly (101) textured when annealed at $T_a \geq$ 1000 °C.

Based on our results we can conclude that the preparation of crystalline and single-phase, thus high-entropy, oxides from equimolar Al–Cr–Nb–Ta–Ti targets show nearly similar chemical compositions and the same rutile-type structure over a rather wide oxygen flow-rate ratio (f_{O2}, which was varied between 30 and 80%) used. Only the growth morphology and total coating thickness slightly depend on f_{O2}, being more dense and columnar-like, but also thinner for higher f_{O2}. Therefore, H and E of our $(Al_{0.19}Cr_{0.13}Nb_{0.19}Ta_{0.30}Ti_{0.19})O_2$ coatings slightly increase from 22 to 24 GPa, and 380–400 GPa, with increasing f_{O2} from 30 to 80%.

The coatings remain with their single-phase crystalline rutile structure up to the maximum annealing temperature of 1200 °C tested. During annealing at T_a = 1000 °C their nearly random crystal orientation changes to a highly 101-texture, causing the hardness to decrease and the indentation modulus to increase, as shown for the coating prepared with f_{O2} = 80%. For this coating, H decreases from 24 to 21 GPa and E increases from 400 to 460 GPa, when T_a increases from 900 to 1000 °C.

Consequently, the high-entropy effect of our $(Al,Cr,Nb,Ta,Ti)O_2$ coatings leads to a significant stabilisation of their rutile structure (being a stable structure for TiO_2, and a metastable one for CrO_2, NbO_2, and TaO_2).

Acknowledgements

The authors acknowledge the use of the X-ray center (XRC) and USTEM at TU Wien. They are also very grateful to Tomasz Wojcik (TU Wien, Austria) for assistance with the TEM investigations and valuable discussions. Plansee Composite Materials GmbH is acknowledged for financial support.

Appendix A. Supplementary data

Supplementary data to this article can be found online at https://doi.org/10.1016/j.vacuum.2019.108850.

References

[1] S. PalDey, S.C. Deevi, Single layer and multilayer wear resistant coatings of (Ti,Al)N: a review, Mater. Sci. Eng. A 342 (2003) 58–79, https://doi.org/10.1016/S0921-5093(02)00259-9.
[2] R. Rachbauer, D. Holec, P.H. Mayrhofer, Increased thermal stability of Ti-Al-N thin films by Ta alloying, Surf. Coat. Technol. 211 (2012) 98–103, https://doi.org/10.1016/j.surfcoat.2011.07.009.
[3] R. Rachbauer, D. Holec, P.H. Mayrhofer, Phase stability and decomposition products of Ti-Al-Ta-N thin films, IEEE Trans. Inf. Theory 39 (1993) 999–1013, https://doi.org/10.1109/18.256506.
[4] L. Chen, Z.Q. Liu, Y.X. Xu, Y. Du, Influence of Zr on structure, mechanical and thermal properties of Cr-Al-N coatings, Surf. Coat. Technol. 275 (2015) 289–295, https://doi.org/10.1016/j.surfcoat.2015.05.004.
[5] S.A. Glatz, R. Hollerweger, P. Polcik, R. Rachbauer, J. Paulitsch, P.H. Mayrhofer, Thermal stability and mechanical properties of arc evaporated Ti–Al–Zr–N hard coatings, Surf. Coat. Technol. 266 (2015) 1–9, https://doi.org/10.1016/j.surfcoat.2015.01.042.
[6] R. Hollerweger, L. Zhou, D. Holec, C.M. Koller, R. Rachbauer, P. Polcik, P.H. Mayrhofer, Controlling microstructure, preferred orientation, and mechanical properties of Cr-Al-N by bombardment and alloying with Ta, J. Appl. Phys. 119 (2016), https://doi.org/10.1063/1.4941533.
[7] C.M. Koller, R. Hollerweger, C. Sabitzer, R. Rachbauer, S. Kolozsvári, J. Paulitsch, P.H. Mayrhofer, Thermal stability and oxidation resistance of arc evaporated TiAlN, TaAlN, TiAlTaN, and TiAlN/TaAlN coatings, Surf. Coat. Technol. 259 (2014) 599–607, https://doi.org/10.1016/j.surfcoat.2014.10.024.
[8] W.M. Seidl, M. Bartosik, S. Kolozsvári, H. Bolvardi, P.H. Mayrhofer, Influence of Ta on the fracture toughness of arc evaporated Ti-Al-N, Vacuum 150 (2018) 24–28, https://doi.org/10.1016/j.vacuum.2018.01.028.
[9] H. Asanuma, F.F. Klimashin, P. Polcik, S. Kolozsvári, H. Riedl, P.H. Mayrhofer, Hard Ti–Al–N endowed with high heat-resistance through alloying with Ta and Ce, Surf. Coat. Technol. 372 (2019) 26–33, https://doi.org/10.1016/j.surfcoat.2019.05.018.
[10] I. Levin, D. Brandon, Metastable Alumina polymorphs: crystal structures and transition sequences, J. Am. Ceram. Soc. 81 (2005) 1995–2012, https://doi.org/10.1111/j.1151-2916.1998.tb02581.x.
[11] C. Ruberto, Metastable Alumina from Theory : Bulk , Surface , and Growth of κ-Al 2 O 3 Metastable Alumina from Theory : Bulk , Surface , and, (2001).
[12] K. Fujishima, A. and Honda, A. Fujishima, K. Honda, © 1972 Nature Publishing Group, Nature 238 (1972) 37, https://doi.org/10.1038/239137a0.
[13] M. Ristić, S. Popović, S. Musić, Structural properties of the system Al2O3Cr2O3, Mater. Lett. 16 (1993) 309–312, https://doi.org/10.1016/0167-577X(93)90198-7.
[14] I. Levin, D. Brandon, Metastable Alumina Polymorphs : Crystal Structures and, 2012, (2012), pp. 1995–2012.
[15] C.M. Koller, V. Dalbauer, A. Kirnbauer, M. Sauer, S. Kolozsvári, J. Ramm, P.H. Mayrhofer, Impact of Si and B on the phase stability of cathodic arc evaporated $Al_{0.70}Cr_{0.30}$-based oxides, Scr. Mater. 152 (2018), https://doi.org/10.1016/j.scriptamat.2018.04.018.
[16] A. Kirnbauer, V. Dalbauer, P. Kutrowatz, S. Kolozsvári, J. Ramm, C.M. Koller, P.H. Mayrhofer, Oxygen dependent morphology and mechanical properties of Al–Cr–(Fe)-based coatings, Surf. Coat. Technol. 349 (2018), https://doi.org/10.1016/j.surfcoat.2018.05.041.
[17] P. Löbl, M. Huppertz, D. Mergel, Nucleation and growth in TiO2 films prepared by sputtering and evaporation, Thin Solid Films 251 (1994) 72–79, https://doi.org/10.1016/0040-6090(94)90843-5.
[18] B. Cantor, I.T.H. Chang, P. Knight, A.J.B. Vincent, Microstructural development in equiatomic multicomponent alloys, Mater. Sci. Eng. A 375–377 (2004) 213–218, https://doi.org/10.1016/j.msea.2003.10.257.
[19] J.-W. Yeh, S.-J. Lin, T.-S. Chin, J.-Y. Gan, S.-K. Chen, T.-T. Shun, C.-H. Tsau, S.-Y. Chou, Formation of simple crystal structures in Cu-Co-Ni-Cr-Al-Fe-Ti-V alloys with multiprincipal metallic elements, Metall. Mater. Trans. A 35 (2004) 2533–2536, https://doi.org/10.1007/s11661-006-0234-4.
[20] J.-W. Yeh, S.-K. Chen, S.-J. Lin, J.-Y. Gan, T.-S. Chin, T.-T. Shun, C.-H. Tsau, S.-Y. Chang, Nanostructured high-entropy alloys with multiple principal elements: novel alloy design concepts and outcomes, Adv. Eng. Mater. 6 (2004) 299–303, https://doi.org/10.1002/adem.200300567.
[21] Nanostructured nitride films of multi-element high-entropy alloys by reactive DC sputtering, Surf. Coat. Technol. 188–189 (2004) 193–200, https://doi.org/10.1016/j.surfcoat.2004.08.023.

[22] P.-K. Huang, J.-W. Yeh, T.-T. Shun, S.-K. Chen, Multi-principal-element alloys with improved oxidation and wear resistance for thermal spray coating, Adv. Eng. Mater. 6 (2004) 74–78, https://doi.org/10.1002/adem.200300507.
[23] J.-W. Yeh, Recent progress in high-entropy alloys, Ann. Chim. Sci. Mater. 31 (2006) 633–648, https://doi.org/10.3166/acsm.31.633-648.
[24] C.H. Lai, S.J. Lin, J.W. Yeh, S.Y. Chang, Preparation and characterization of AlCrTaTiZr multi-element nitride coatings, Surf. Coat. Technol. (2006), https://doi.org/10.1016/j.surfcoat.2006.06.048.
[25] C.-H. Lai, M.-H. Tsai, S.-J. Lin, J.-W. Yeh, Influence of Substrate Temperature on Structure and Mechanical, Properties of Multi-Element (AlCrTaTiZr)N Coatings, (2007), https://doi.org/10.1016/j.surfcoat.2007.01.001.
[26] K.H. Cheng, C.H. Weng, C.H. Lai, S.J. Lin, Study on adhesion and wear resistance of multi-element (AlCrTaTiZr)N coatings, Thin Solid Films (2009), https://doi.org/10.1016/j.tsf.2009.03.139.
[27] S.-Y. Chang, M.-K. Chen, D.-S. Chen, Multiprincipal-element AlCrTaTiZr-nitride nanocomposite film of extremely high thermal stability as diffusion barrier for Cu metallization, J. Electrochem. Soc. (2009), https://doi.org/10.1149/1.3097186.
[28] R. Hahn, A. Kirnbauer, M. Bartosik, S. Koloszvári, P.H. Mayrhofer, Toughness of Si alloyed high-entropy nitride coatings, Mater. Lett. (2019), https://doi.org/10.1016/j.matlet.2019.05.074.
[29] M.I. Lin, M.H. Tsai, W.J. Shen, J.W. Yeh, Evolution of structure and properties of multi-component (AlCrTaTiZr)Ox films, Thin Solid Films 518 (2010) 2732–2737, https://doi.org/10.1016/j.tsf.2009.10.142.
[30] X. Liu, G.J. Ma, G. Sun, Y.P. Duan, S.H. Liu, Effect of deposition and annealing temperature on mechanical properties of TaN film, Appl. Surf. Sci. 258 (2011) 1033–1037, https://doi.org/10.1016/j.apsusc.2011.08.116.
[31] P.H. Mayrhofer, A. Kirnbauer, P. Ertelthaler, C.M. Koller, High-entropy ceramic thin films; A case study on transition metal diborides, Scr. Mater. 149 (2018) 93–97, https://doi.org/10.1016/j.scriptamat.2018.02.008.
[32] C.M. Rost, E. Sachet, T. Borman, A. Moballegh, E.C. Dickey, D. Hou, J.L. Jones, S. Curtarolo, J.P. Maria, Entropy-stabilized oxides, Nat. Commun. 6 (2015) 1–8, https://doi.org/10.1038/ncomms9485.
[33] K. Chen, X. Pei, L. Tang, H. Cheng, Z. Li, C. Li, X. Zhang, L. An, A five-component entropy-stabilized fluorite oxide, J. Eur. Ceram. Soc. 38 (2018) 4161–4164, https://doi.org/10.1016/j.jeurceramsoc.2018.04.063.
[34] A. Sarkar, R. Djenadic, D. Wang, C. Hein, R. Kautenburger, O. Clemens, H. Hahn, Rare earth and transition metal based entropy stabilised perovskite type oxides, J. Eur. Ceram. Soc. 38 (2018) 2318–2327, https://doi.org/10.1016/j.jeurceramsoc.2017.12.058.
[35] T.W. Barbee, W.H. Holmes, D.L. Keith, K. Mitchell, Gheorghe ilonca 45 (1977) 591–599.
[36] P.H. Mayrhofer, C. Mitterer, L. Hultman, H. Clemens, Microstructural design of hard coatings, Prog. Mater. Sci. 51 (2006) 1032–1114, https://doi.org/10.1016/j.pmatsci.2006.02.002.
[37] W.C. Oliver, G.M. Pharr, An improved technique for determining hardness and elastic modulus using load and displacement sensing indentation experiments, J. Mater. Res. 7 (1992) 1564–1583, https://doi.org/10.1557/JMR.1992.1564.